Chain Orientation in Block Copolymers Exhibiting Cylindrically Confined Crystallization

Daniel J. Quiram† and Richard A. Register*

Department of Chemical Engineering, Princeton University, Princeton, New Jersey 08544

Gary R. Marchand‡

The Dow Chemical Company, P.O. Box 400, Plaquemine, Louisiana 70765

Douglas H. Adamson

Princeton Materials Institute, Princeton University, Princeton, New Jersey 08544

Received August 12, 1997; Revised Manuscript Received March 16, 1998

ABSTRACT: The orientation of the crystal stems in diblock copolymers, where crystallization occurs within the cylindrical microdomains present in the melt mesophase, is investigated via X-ray scattering on flow-aligned specimens. A series of ethylene-*b*-(3-methyl-1-butene) diblocks (E/MB) is compared with an ethylene-*b*-(vinylcyclohexane) diblock (E/VCH), where MB is rubbery ($T_g < T_{room}$) and VCH is vitreous ($T_g = 134$ °C) at the freezing point of the E block. All of the diblocks contain 26−28 wt % E, leading to a morphology of hexagonally-packed E cylinders. Crystallization in all of these materials can be confined to the cylindrical microdomains. Not only do the crystals align preferentially within the semicrystalline cylinders, but this orientation varies depending on the ability of chains to diffuse during the crystallization process. When chain diffusion is most rapid, alignment is observed with the chain axis in the crystals perpendicular to the cylinder axis and the *b* axis (fast growth axis) coincident with the cylinder axis. However, when the chain mobility is limited, the crystal stems tilt with respect to a plane which is normal to the cylinder axis, allowing better accommodation of amorphous material at the crystallite surface.

Introduction

Crystallization is a widely studied phenomenon which imparts important physical properties to polymeric materials. In this decade, detailed studies of block copolymers containing a crystallizable component have begun to emerge.[1−17] In such materials, crystalline structure formation is complicated by the fact that microphase separation in the melt can result from block incompatibility prior to crystallization. Initial studies investigating crystallization from both homogeneous[1−3] and weakly segregated[3−5] block copolymer melts concluded that a lamellar morphology resulted upon solidification, regardless of any prior melt structure.

We recently examined[6,7] the interaction between crystallization and microphase segregation in a series of ethylene-*b*-(3-methyl-1-butene) diblocks (E/MB) of constant composition (E weight fraction $f_E = 0.26-0.27$) and varying molecular weight. Through small-angle X-ray scattering (SAXS) experiments on the highest molecular weight materials, having order−disorder transition temperatures $T_{ODT} > 260$ °C, we demonstrated that strong segregation could confine crystallization to preestablished cylindrical microdomains, even when both blocks were well above their glass transitions at the crystallization temperature and the crystallization rate was slow. When the melt was weakly segregated ($T_{ODT} = 167$ °C), crystallization could be confined to the cylinders provided that the crystallization rate was sufficiently high, while at slower rates a lamellar morphology resulted. Here, we investigate the chain orientation within cylindrical microdomains in the E/MB series and compare it with that of an ethylene-*b*-(vinylcyclohexane) diblock (E/VCH; $f_E = 0.28$), where vitrification of the matrix block (VCH $T_g = 134$ °C) confines crystallization to cylinders.

The direction of chain folding, or the orientation of the crystal stems, within semicrystalline block copolymer microdomains is a topic which has been investigated by several groups,[1,4,8−15,18,19] all studying materials with lamellar microdomain structures. Rangarajan *et al.*[1,2] inferred that the E chain axis lies normal to the lamellar interface for ethylene-*b*-(ethylene-*alt*-propylene) diblock copolymers (E/EP) crystallizing from homogeneous melts, on the basis of the presence of spherulites in the solid state. Yang and co-workers[8] observed this same orientation on the basis of SAXS and Raman spectroscopy measurements for low-molecular-weight block copolymers containing ethylene oxide (EO) which crystallized from single-phase or weakly segregated melts. Conversely, through pole figure analysis on aligned samples, Cohen and co-workers[9] found that the E chain axis runs parallel to the domain interface in ethylene-*b*-(ethylethylene) diblocks (E/EE) which crystallize from heterogeneous melts. More recently, Hamley *et al.*[10,11] observed this same chain orientation in lamellar E/EE, E/EP, and E/VCH diblocks through two-dimensional wide-angle X-ray scattering (2D WAXS) on shear-oriented samples. Thus, in lamellar systems, the stem orientation appears to vary depending on the state of the material (homogeneous, microphase-separated, partially vitrified) at the crystallization conditions.

We have previously shown[6] that, for our highest molecular weight E/MB diblock (88 kg/mol, see Table

* To whom correspondence should be addressed.
† Present address: The Procter & Gamble Company, Winton Hill Technical Center, Cincinnati, OH 45224.
‡ Present address: Dow−DuPont Elastomers L.L.C., P.O. Box 400, Plaquemine, LA 70765-0400.

S0024-9297(97)01218-7 CCC: $15.00
Published on Web 07/03/1998

Table 1. Block Copolymer Characteristics

sample	M_w (kg/mol)	f_E	T_{ODT} (°C)	E T_m (°C)	E w_c	E T_c at 10 °C/min (°C)	E T_c at 20 °C/min (°C)	cylinder radius at 23 °C (nm)
E/MB44	44.3	0.26	167	105	0.31	71	64	9.8
E/MB63	62.7	0.27	>260	105	0.28	62	61	14
E/MB88	87.9	0.27	>260	103	0.26	62	61	16
E/VCH36	35.8	0.28	>260	106	0.25	62	60	8.0

Chart 1. Chemical Structures of E, MB, and VCH Blocks

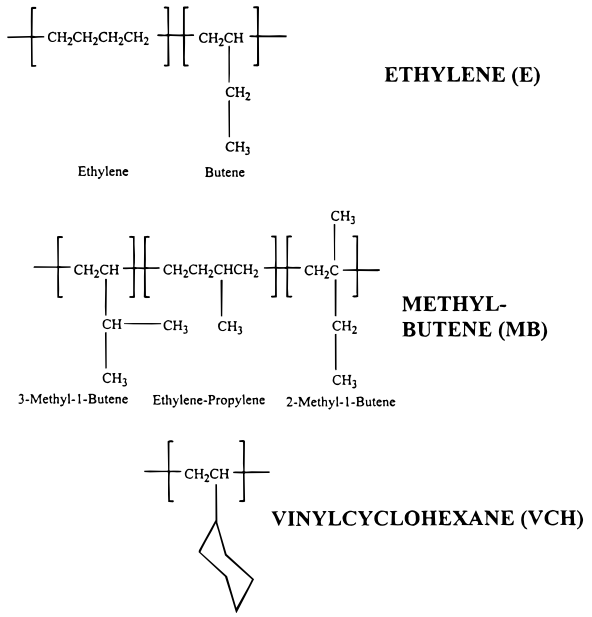

1), crystallization on cooling from the melt at 10−20 °C/min leads to a crystal stem orientation roughly normal to the cylinder axis, though with some tilt. Since this orientation was unexpected and since the orientation of crystal stems within cylindrical microdomains had not been previously explored (in contrast to the lamellar case), we present here a more thorough examination of this cylindrically confined crystallization, in cases where the matrix block is both above and below its glass transition temperature during crystallization of the block forming the cylinders.

Experimental Section

The E/MB precursors (high-1,4 butadiene)-*b*-(high-3,4 isoprene) were synthesized via sequential anionic polymerization in cyclohexane; detailed descriptions of the synthesis, molecular characterization, and hydrogenation are given elsewhere.[6,20] The E/VCH precursor, (high-1,4 butadiene)-*b*-styrene (B/S), was anionically-synthesized using standard high-vacuum techniques[21] in a 90/10 v/v cyclohexane/benzene mixture at room temperature, with *tert*-butyllithium as the initiator and tetrahydrofuran used to speed the crossover reaction. Molecular characterization of the E/VCH precursor was performed using ^{1}H nuclear magnetic resonance and gel permeation chromatography. Hydrogenation to yield E/VCH36 was conducted in cyclohexane employing a heterogeneous Pd^0 catalyst supported on $CaCO_3$ (5% Pd^0; Strem) to saturate both blocks.[22,23] Fourier transform infrared spectroscopy (FTIR) was used to verify that both blocks were saturated to the detectability limits (>98% of the B block; >99% of the S block). The chemical structures of the saturated derivatives are shown in Chart 1. For the E/MB series, the MB microstructure varies slightly between samples, as described in detail previously;[6] the average content of 3-methyl-1-butene/ethylene-propylene/2-methyl-1-butene units is 50:42:8. Other relevant characteristics appear in Table 1; diblocks are denoted by the block chemistry and the molecular weight of the saturated polymer in kilograms per mole. All polymers have $f_E = 0.26-0.28$ and $M_w/M_n < 1.1$. Order−disorder transition temperatures (T_{ODT}s) were measured as described previously.[24] Final melting temperatures (T_m) on heating, peak crystallization temperatures (T_c) on cooling, and the VCH glass transition temperature (T_g) on heating were determined using a Perkin-Elmer DSC-7 calibrated with indium and mercury. The weight fraction crystallinity of the E blocks (w_c) in fast cooled (see below) samples, normalized by f_E, was calculated from the DSC heating runs on the basis of a theoretical value of 277 J/g[25] for 100% crystalline polyethylene (see Table 1). Both dynamic cooling and isothermal crystallization runs were performed with the DSC-7 to obtain values for the crystallization half-times, $t_{1/2}$, listed in Table 2. Cylinder radii were calculated at room-temperature on the basis of the volume fraction of E block and the domain spacing measured by SAXS for materials which were fast cooled (see below);[6,20] the weight fraction crystallinity was determined via DSC,[6] and room-temperature densities were taken from the literature: 0.856 g/cm^3 (E, amorphous),[26] 0.986 g/cm^3 (E, crystalline),[27] 0.863 g/cm^3 (MB),[26] and 0.950 g/cm^3 (VCH).[28]

Flow-induced alignment of these materials was achieved using a lubricated channel die based on the design of Khan and Larson.[29] Molding[30] was performed at 150 °C (E/MB diblocks) or 180 °C (E/VCH), using compression ratios ranging from 5.8 to 7.8 (with the exception of 11 used for E/MB88 FC; see Table 2) and holding the processed strip in the die at the molding temperature for 15 min before cooling. "Fast cooled" (FC) specimens were cooled from the 140−150 °C melt at 10−20 °C/min. E/MB63 and E/MB88 were also "slow cooled" (SC) and crystallized at an intermediate temperature (T_c; 77 °C for E/MB63, 71 °C for E/MB88); however, note that cooling from 100 °C to T_c in the hot press required 45 min, so some crystallization may have occurred at T slightly greater than T_c. A strip of E/MB44 was "quenched" (Q) by removing the channel die from the hot press after annealing and submerging it in a large beaker of ice water. E/VCH36 was cooled at ∼0.5 °C/min down to room temperature ("very slow cooled", VSC); faster cooling rates led to cracking in this brittle material. Crystallization half-times ($t_{1/2}$) determined by DSC are listed in Table 2, where the DSC was operated so as to emulate the thermal history experienced by specimens in the channel die.

Simultaneous 2D SAXS and WAXS were performed on the oriented samples using a Philips XRG-3000 sealed tube generator with a Cu target, a Huber 151 graphite monochromator (adjusted for Cu Kα radiation), an evacuated Statton pinhole camera (W.H. Warhus), and Kodak image plates read with a Molecular Dynamics Phosphorimager SI scanner. A hole was cut in the middle of the upstream image plate used to collect WAXS, allowing the main beam and SAXS to pass through to the beam stop and the second (SAXS) image plate. From the digitized WAXS patterns, azimuthal traces of E unit cell reflections were generated in order to examine the unit cell orientation. Data from the 2D WAXS images (averaged over 2−4 runs on each sample) are listed in Table 2.

Results and Discussion

E/MB44 is the lowest molecular weight material exhibiting cylindrically confined crystallization. 2D SAXS and WAXS images for E/MB44 FC are shown in Figure 1. Though the orientation of the cylinders seen by SAXS is not as good as that for the specimens shown later in this paper, the six spots visible at the points of a regular hexagon (see arrows in Figure 1a) when the X-ray beam is along the channel die flow direction (FD)

Table 2. 2D WAXS Results on Oriented Specimens

polymer	thermal history	comp ratio	$t_{1/2}$ (min)	avg (110) sep angle (deg)	avg tilt angle[a] (deg)	tilt angle range[b] (deg)	avg (110) fwhm[c] (deg)	avg (200) fwhm[c] (deg)
E/MB44	Q	7.7	<0.1	114 ± 3	9	0−14	36 ± 4	68 ± 11
E/MB44	FC	5.8	0.7	117 ± 2	0	0−6	20 ± 3	22 ± 4
E/MB63	FC	7.4	0.6	119 ± 3	0	0	39 ± 6	45 ± 13
E/MB63	SC	7.0	5	118 ± 2	0	0	23 ± 1	22 ± 3
E/MB88	FC	11	0.5	108 ± 3	18	14−21	38 ± 9	80 ± 13
E/MB88	SC	6.9	5	120 ± 4	0	0	33 ± 8	35 ± 6
E/VCH36	VSC	7.8	8	99 ± 2	26	25−28	22 ± 3	112 ± 4

[a] Tilt angle of crystal stem relative to a plane which is normal to the cylinder axis, assuming all tilt is around the *a* axis of E crystals (model of Figure 4b). [b] Tilt angle range based on the standard deviation of the (110) separation angle. [c] Azimuthal full width at half of the maximum peak intensity.

indicate a hexagonal packing of cylinders with their axes along the FD. For all materials studied here, SAXS images taken with the beam along either the loading direction (LD) or the constraint direction (CD) showed two spots on the equator, as expected for cylinders with their axes along the FD. The SAXS pattern of Figure 1a shows that the cylinders are oriented such that (11) planes are perpendicular to the elongation plane. For E/MB88 FC, we noted previously[6] that either the (11) or (10) planes could be normal to the elongation plane and that both orientations have been found in different parts of a single processed strip. Note, however, that the orientation must be of one preferred type over the region illuminated by the X-rays (0.1 mm diameter × 2.5 mm thickness) for a distinct six-spot pattern to be visible. Large-amplitude oscillatory shear has also been shown[31] to orient either the (11) or the (10) planes normal to the flow-vorticity plane, depending on the proximity of the processing temperature to T_{ODT}. The crystallites situated in the cylinders should, as an ensemble, show cylindrical symmetry, so the informative WAXS images have the beam oriented perpendicular to the cylinders (along either the LD or the CD). With such cylindrical symmetry, both possible microdomain orientations—(11) or (10) planes normal to the elongation plane—produce identical 2D WAXS. The cylindrical symmetry was confirmed by pole figure analysis (see Acknowledgment) of the (110) and (200) polyethylene wide-angle reflections from samples E/MB44 FC and E/VCH36 VSC.

In the 2D WAXS image for E/MB44 FC shown in Figure 1b (and others shown below), the beam is along the LD and the cylinders are aligned vertically with respect to the image plate. There are three rings evident in this image: the unoriented, broad inner ring due to scattering from amorphous segments and two oriented outer rings corresponding to the (110) and (200) reflections of the orthorhombic E unit cell. The (110) reflection displays four off-axis regions of high intensity, while the (200) reflection shows intense regions on the equator. The image with the beam directed along the CD appears similar to that shown in Figure 1b, while the image with the beam along the FD displays weak isotropic rings for the (110) and (200) reflections (true for all samples examined here). If the chain axis were aligned parallel to the cylinder axis (see Figure 2a), as might be suggested by the findings for crystallization from strongly segregated lamellar melts,[9−12] a standard fiber pattern would result with all (*hk*0) reflections situated on the equator. However, if the chain axis were aligned perpendicular to the cylinder axis (see Figure 2b), with *b*-axial orientation, an image similar to that observed for E/MB44 FC would result in which the (110) maxima would be separated by an azimuthal angle of 116° across the equator. The measured (110) azimuthal separation angle (σ) for E/MB44 FC is 117 ± 2° (average from two images; see Table 2), within experimental uncertainty of 116°. From Table 2, σ for E/MB44 Q is measured to be 114 ± 3°, also within experimental uncertainty of 116°. Thus, the chain stems are preferentially aligned normal to the cylinder axis (as in Figure 2b) in E/MB44, regardless of thermal history. This type of unit cell orientation is likely to be the most prevalent because it allows the crystallites to grow long in one direction; the *b* dimension of the unit cell (fast growth direction for polyethylene homopolymers[32]) is coincident with the cylinder axis. While crystallites in a variety of orientations can nucleate and grow, as evidenced by the nonzero intensity of the (110) reflection even on the meridian and equator, it is the crystallites with the orientation shown in Figure 2b which grow the longest and therefore dominate the structure and the X-ray scattering patterns. Small-angle X-ray scattering from the crystallites within the cylinders, as observed for crystallites within lamellar microdomains,[1,3,4] is particularly evident when the cylinders are larger (E/MB63 and E/MB88, see Table 1). The crystallites produce SAXS intensity most intense on the equator, consistent with the model shown in Figure 2b, indicating that the crystals are much longer along the cylinder axis than transverse.

Values calculated for the azimuthal full width at half of the maximum intensity (fwhm) for both the (110) and (200) reflections are also listed in Table 2. These were calculated by first subtracting a baseline (based on average intensity values on the meridian) from the given reflection and then determining the width of the high-intensity regions (in azimuthal degrees) where the intensity is half that of the peak. Note that the intensity of the (110) on the meridian, while small, is generally not zero; therefore, this subtracted background also includes a small unoriented crystal component in addition to the amorphous scattering. Four values were averaged together for the (110) reflection, and two, for the (200) reflection from each image. The azimuthal fwhm values provide a means to compare the degree of orientation between samples. From Table 2, it can be seen that both fwhm values for E/MB44 FC are less than those for E/MB44 Q. Since the degree of alignment of the cylinders for E/MB44 Q, as seen by SAXS, is actually slightly better than that for E/MB44 FC,[20] this indicates that there is superior alignment of the crystal stems in E/MB44 FC.

Images for E/MB63 FC are shown in Figure 3 and bear a strong resemblance to those for E/MB44 in Figure 1. Oriented hexagonally-packed cylinders are evident from SAXS, while a σ value of 119 ± 3° is seen in the WAXS image. From Table 2, E/MB63 SC (crystallized

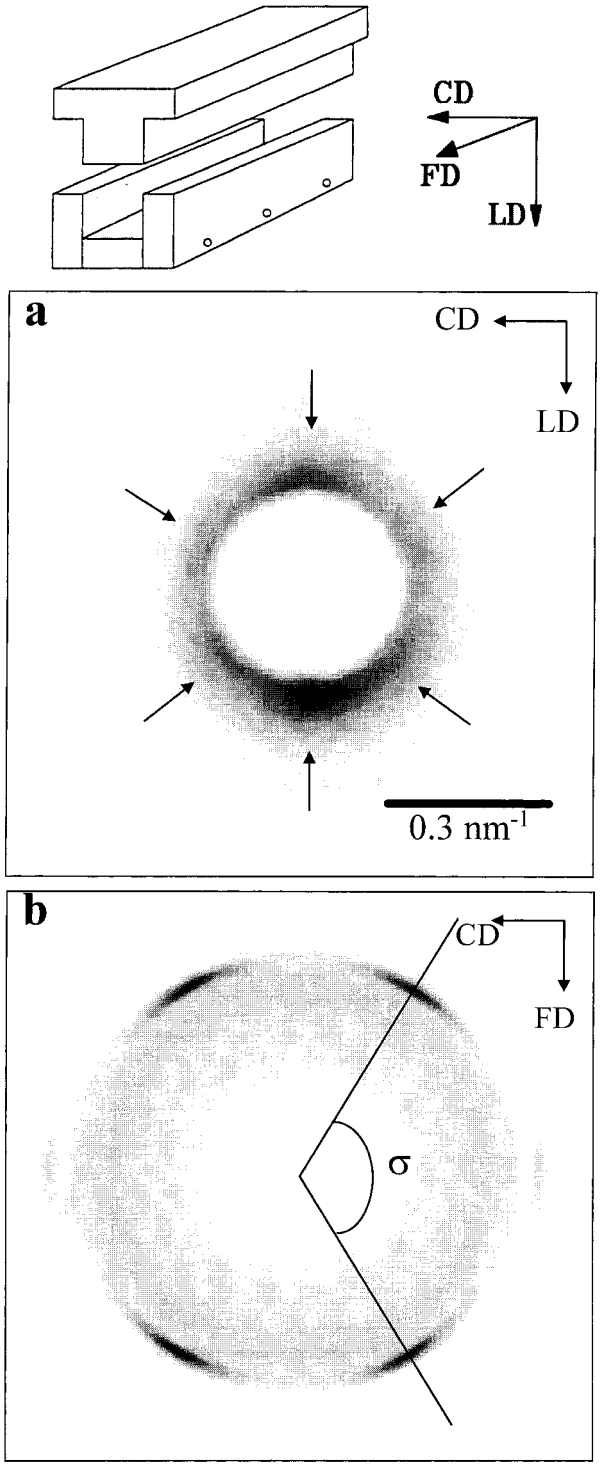

Figure 1. (top) Schematic diagram of the channel die used for specimen alignment, with the three principal directions indicated: flow direction (FD), constraint direction (CD), and loading direction (LD). (a) 2D SAXS image acquired on an aligned, crystallized specimen of E/MB44 FC at room temperature. The X-ray beam is along the FD, with the CD and the LD labeled. (b) 2D WAXS image acquired on a similar sample of E/MB44 FC at room temperature. In this case, the X-ray beam is along the LD, with the CD and the FD labeled; thus, the cylinder axis is vertical with respect to this image. The diffuse inner ring is the unoriented amorphous halo. With increasing scattering angle, the first crystalline reflection is due to the (110) planes of orthorhombic polyethylene and displays four off-axis regions of high intensity, making an azimuthal angle σ about the equator. At slightly higher scattering angle, a second crystalline reflection, (200), is preferentially located on the equator.

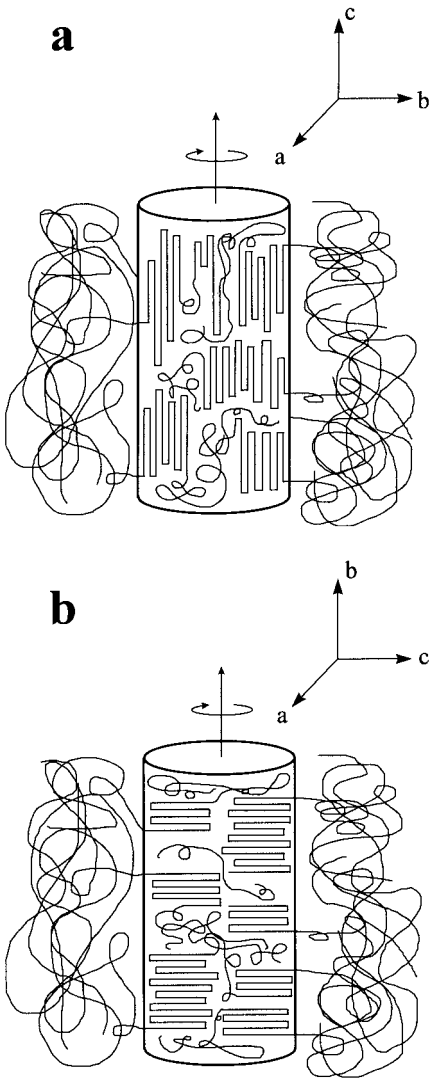

Figure 2. Schematic diagrams of two possible chain orientations which might be observed for cylindrically confined crystallization in block copolymer systems. The unit cell directions are labeled next to each of the diagrams. (a) Chains are oriented parallel to the cylinder axis. (b) Chains are oriented perpendicular to the cylinder axis. Cylindrical symmetry (rotation around the cylinder axis) is presumed in both cases.

at 77 °C) has a σ value of 118 ± 2°. Both of these values are close to 116° and are therefore indicative of an orientation in which the crystal stems are normal to the cylinder axis, regardless of the crystallization conditions. From the (110) and (200) azimuthal fwhm values (see Table 2), it is apparent that there is substantially better orientation of the crystal stems in E/MB63 SC than in E/MB63 FC. The crystallization process is significantly slower for SC ($t_{1/2} \approx 5$ min, see Table 2) than for FC; thus, as found for E/MB44 above, slower crystallization results in better stem orientation.

By contrast, our previous 2D WAXS image[6] on oriented E/MB88 FC shows that the (110) azimuthal peaks were separated by an angle of 108 ± 3° across the equator (see Table 2). This value of σ is significantly different from the 116° expected for the model of Figure 2b. There are two types of unit cell tilt (relative to the orientation shown in Figure 2b) which would account for a σ value less than 116°. The first possibility is a tilt around *c* (see Figure 4a). Strictly speaking, this would cause each of the four (110) azimuthal high-

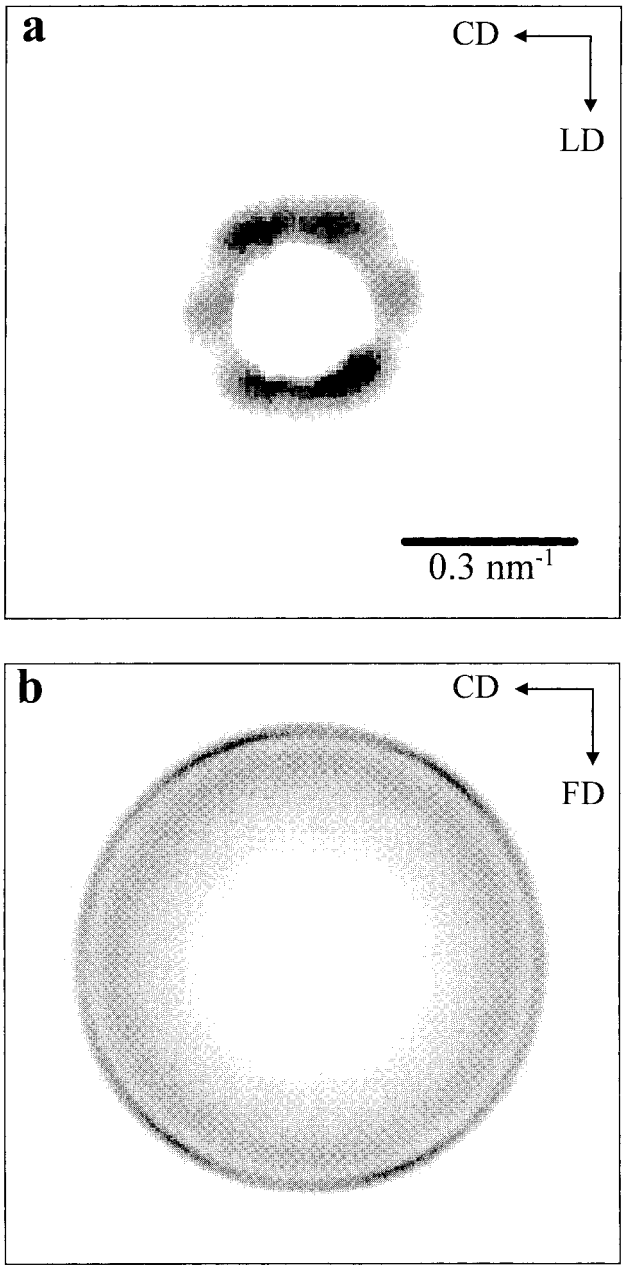

Figure 3. (a) 2D SAXS image acquired on an aligned, crystallized specimen of E/MB63 FC at room temperature. The X-ray beam is along the FD, with the CD and the LD labeled. (b) 2D WAXS image acquired on a similar sample of E/MB63 FC at room temperature. In this case, the X-ray beam is along the LD, with the CD and the FD labeled; thus, the cylinder axis is vertical with respect to this image.

intensity regions to split into two regions of high intensity (eight total). For example, if all crystals had their *b* axes rotated by 70° from the cylinder axis ($\alpha = \pm 70°$), then the (110) azimuthal maxima would display σ values of 110° and 28°, respectively.[33,34] Tilt around *c* would also cause the (200) reflection to appear as four off-axis azimuthal maxima with an angle of separation across the equator approximately equal to twice the tilt angle (148° for $\alpha = \pm 70°$). For continuous distributions of α, the (110) peak could retain its four-spot character, but the spots would broaden and move relative to the idealized case drawn in Figure 2b, while the (200) peak would appear as two arcs centered on the equator. Indeed, as discussed below, very broad (200) arcs are found for the samples showing the most extensive tilt.

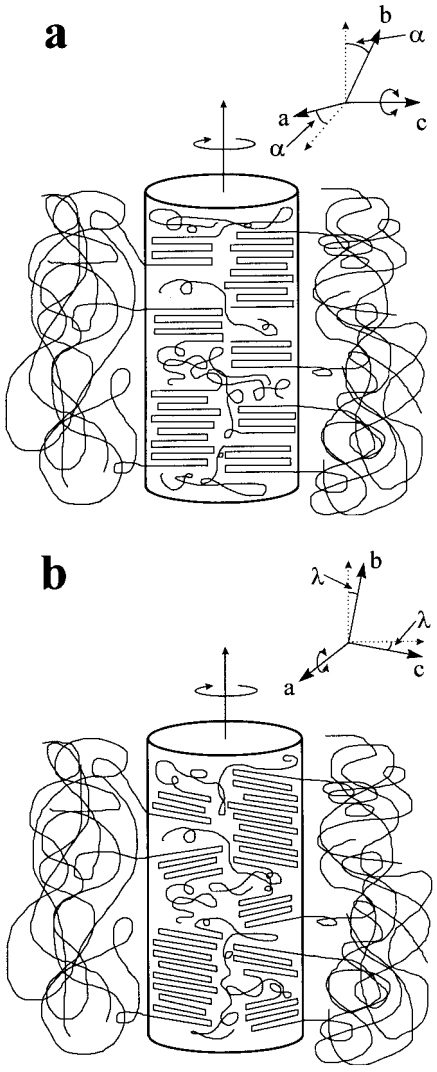

Figure 4. Schematic diagrams of two possible types of unit cell tilt which could yield (110) azimuthal separation angles less than 116°. The unit cell directions are labeled next to each of the diagrams. (a) Tilt around *c* by an angle α. (b) Tilt around *a* by an angle λ, which results in tilting of the chains with respect to a plane which is normal to the cylinder axis. Note that there is cylindrical symmetry (rotation around the cylinder axis) in both cases.

A second possible cause for the (110) high-intensity regions moving toward the equator is the tilt around *a*, in other words, tilting of the chains with respect to a plane which is perpendicular to the cylinder axis (see Figure 4b). The σ value of 108 ± 3° corresponds to chains preferentially tilted at an angle of 18 ± 4°, as noted previously.[6] Since tilt around *a* does not affect the (200) planes, the (200) scattering will still be situated on the equator. Since both types of tilt may actually occur, and their effects on the 2D WAXS patterns are not entirely dissimilar, it is difficult to gauge how much of each type of tilt is present given that only the (110) and (200) reflections are sufficiently intense to permit analysis. For approximate quantification of the amount of tilt, we will adopt the model shown in Figure 4b, as this provides a direct relationship between σ and the tilt angle λ, whereas use of the model in Figure 4a would require additional assumptions about the distribution of tilt angles α. For the discussion presented below, knowledge of the exact type and distribution of tilt is not required, only an indication of

how the extent of tilt changes with the material type and processing history.

SAXS and WAXS images for E/MB88 SC (crystallized at 71 °C) appear quite similar to those shown for E/MB63 FC in Figure 3. The σ value of 120 ± 4° (see Table 2) corresponds to the crystal stems aligned perpendicular to the cylinder axis. Slight misalignment of either the specimen (X-ray beam not precisely along the LD) or the cylinders within the specimen (cylinder axis not precisely perpendicular to the LD)[34] can result in σ values greater than 116°; the observed $\sigma = 120 \pm 4°$ is best interpreted as reflecting crystal stems perpendicular to the cylinder axis (no tilt). Thus, for E/MB88, slow cooling ($t_{1/2} \approx 5$ min, see Table 2) results in no tilt, while fast cooling produces a preferred tilt near 18°, if all the tilt were around *a*. However, the broad (200) reflection for E/MB88 indicates some tilt around *c* as well.

The results for the three E/MB materials studied can all be organized by noting the correlation between the degree of orientation, the chain mobility, and the rate of crystallization. Crystallization necessarily requires diffusion of the crystallizable block; however, in these segregated block copolymers, one end of the block is preferentially located at the domain interface. Therefore, as the molecular weight of the diblock increases, movement of the crystallizable block becomes progressively more hindered, both by its own increased molecular weight and by the increased tendency for the block junction to be located at the microdomain interface. While we do not have direct information on the rate of diffusion along the cylinder axis, our previous SAXS measurements[6,20] provide some insight into the rate of diffusion transverse to the cylinder axis. For E/MB88 on slow cooling, chain diffusion was sufficiently rapid for the intercylinder spacing to equilibrate prior to crystallization; that is, the spacing at the crystallization temperature is simply that extrapolated from the melt. By contrast, when E/MB88 is fast-cooled, the intercylinder spacing is smaller than that predicted from the melt extrapolation, implying that limited chain diffusion could occur prior to crystallization. For E/MB63 and E/MB44, even fast-cooled specimens had an intercylinder spacing close to the value extrapolated from the melt.

The specimen which showed the best orientation of the crystal stems with respect to the cylinder axis was E/MB44 FC, which has a low molecular weight and was crystallized at a modest rate. The quenched sample, E/MB44 Q, showed a qualitatively similar but poorer orientation (broader azimuthal spread of (110) peaks). The same trend is observed in E/MB63 crystallized at different rates, but the increased molecular weight over E/MB44 means that slower crystallization is required to obtain the same degree of orientation. Thus, the azimuthal (110) spreads (see Table 2) are similar for E/MB63 FC and E/MB44 Q, and E/MB63 SC and E/MB44 FC. Increasing the molecular weight further, E/MB88 SC still shows a perpendicular orientation of the stem against the cylinder axis, but with a degree of orientation closest to that for E/MB63 FC. Finally, E/MB88 FC shows a strong preferred tilt of the *b* axis away from the cylinder axis (18° if all tilt were around *a*). This sequence of observations suggests that the preferred orientation of the crystal stems is perpendicular to the cylinder axis but that if crystallization occurs "too fast" relative to the rate of diffusion of the polymer chains, the crystal stems tilt.

A possible explanation for the observed chain tilt lies in the area per stem at the crystal fold surface. Assuming that the fold surface is still parallel to the cylinder axis when the chains tilt, then tilting increases the area per stem. This larger area provides for better accommodation of the noncrystallizable material at the crystal surface. In the block copolymer case, each chain has a very large "defect"—the amorphous block, which here has nearly triple the molecular weight of the crystallizable block. It may be that, during slow crystallization, the area which needs to be accommodated at the crystal surface is reduced, either through more regular chain folding or through some distortion of the amorphous block. However, when crystallization is fast, this area can only be accommodated by tilting the stems relative to the crystallite surface.

While this report is the first on the cylindrical case, chain tilt relative to a lamellar interface has been previously observed in oligomeric E/EO nonionic surfactants,[13,18,19] where both blocks are crystalline. Through X-ray scattering and Raman spectroscopy, chain tilt of either the E chains (30° tilt angle relative to the lamellar normal)[13] or the EO chains (40−60°)[18,19] has been found in different oligomers. This is thought to result from differences in the cross-sectional area per chain between the two blocks.[13] In our case, the cross-sectional area for the crystalline E stems (based on the E unit cell[27]) is 18.6 Å^2; assuming the same backbone C−C bond lengths and angles for VCH and MB as for E, chain cross-sectional areas of 76 Å^2 for VCH and 36−39 Å^2 for MB (depending on the particular microstructure of the polyisoprene precursor) are calculated from the density values given in the Experimental Section. Tilt angles ranging from 18−45° with respect to the lamellar interface normal have also been determined in the crystallization of low-molecular-weight linear E homopolymers.[35−37] It is unclear how these studies, which are concerned with oligomers, relate to higher molecular weight block copolymers, since oligomeric systems often form extended chain crystals (or crystals with 1−2 folds per chain) and are highly crystalline whereas the E blocks in our polymers are only about 28% crystalline (see Table 1). Here, defects with a much less specific size than that in the E/EO case must be accommodated, and the mismatch in chain cross-sections between the amorphous and crystalline blocks can be compensated for by folding of the crystalline block. Thus, there is little previous experimental work which is clearly relevant to the experimental results presented here.

To determine the influence of vitrification of the matrix block on E chain orientation within cylinders, E/VCH36 was examined. Since the T_g of VCH is 134 °C, the matrix block is vitreous during crystallization of the E block (see T_c values in Table 1). Therefore, this is an even more extreme case than E/MB88 FC, where chain diffusion is severely limited. SAXS and WAXS images for very slow cooled E/VCH36 are shown in Figure 5. The main amorphous halo is particularly intense in this VCH-containing diblock, and an additional inner halo is observed in the 2D WAXS image at $2\theta \approx 8-9°$, which is likely due to correlations between the cyclohexyl rings in the VCH block; this "polymerization ring" has been previously studied in polystyrene.[38]

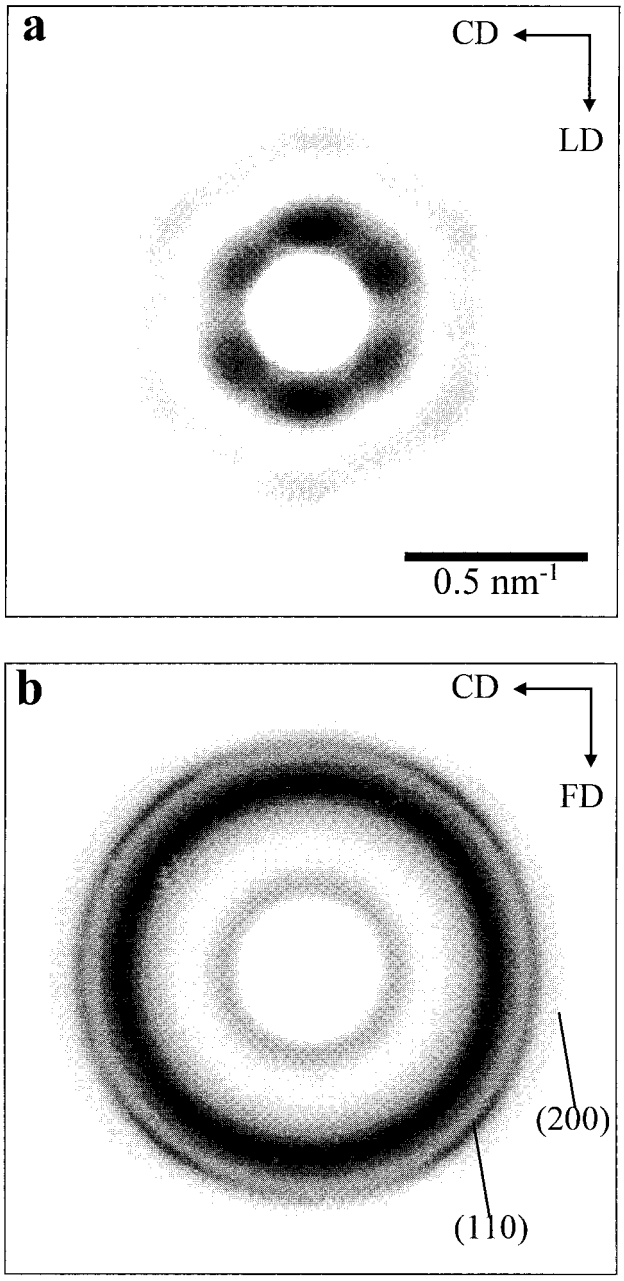

Figure 5. (a) 2D SAXS image acquired on an aligned, crystallized sample of E/VCH36 VSC at room temperature. The X-ray beam is along the FD, with the CD and the LD labeled. The more regular domain structure in E/VCH36 (versus the E/MB diblocks) yields discernible second- and third-order reflections (at scattering vector ratios of $\sqrt{3}$ and $\sqrt{4}$ relative to the primary peak, respectively). The $\sqrt{3}$ spots occur at $(30 + 60n)°$ from the meridian, while the $\sqrt{4}$ spots occur at $60n°$ ($n = 0-5$). Spots corresponding to the $\sqrt{7}$ peak are also observable in the original image. The SAXS pattern with the beam along the CD (not shown) shows two spots on each half of the equator, in a scattering vector ratio of 1:2. (b) 2D WAXS image acquired on a similar sample of E/VCH36 VSC at room temperature. In this case, the X-ray beam is along the LD, with the CD and the FD labeled; thus, the cylinder axis is vertical with respect to this image. The (110) reflection (four off-axis azimuthal maxima) and the (200) reflection (two broad equatorial maxima) from crystalline E are labeled.

A σ value of 99 ± 2° is measured for E/VCH36 (see Table 2). If the σ value were solely due to tilt around *a*, then it would correspond to chains tilted at an angle of 26 ± 2° from a plane which is normal to the cylinder axis (see Figure 4b). From Table 2, the (110) azimuthal fwhm value is low, but the (200) azimuthal fwhm value is extremely high, the highest of any of the materials investigated. In fact, the azimuthal (200) high-intensity regions are plateaus rather than peaks, though there is no indication of splitting of each plateau into two regions of high intensity. To obtain a (200) reflection with such broad arcs on the equator, a mixture of chain tilt from a plane normal to the cylinder axis and tilt around *c* is most likely present. Since rotation around *c* affects the location of the (110) azimuthal maxima, the most prevalent tilt angle may differ slightly from the calculated 26°, but it is clear that the crystals in E/VCH36 depart the most from the orientation shown in Figure 2b. Because the VCH matrix is vitreous throughout crystallization of the E block, chain diffusion in this material is extremely limited, and it shows the largest degree of tilting of any material studied. This supports the connection noted above between the crystal stem orientation and the rate of chain diffusion during crystallization.

Conclusions

When chain diffusion is sufficiently fast relative to crystallization, the polyethylene crystal stems in cylindrical block copolymer microdomains orient perpendicular to the cylinder axis. The predominant orientation of the unit cells is with the *b* axis along the cylinder axis; since the *b* axis is known to be the fast growth direction in polyethylene homopolymers, those crystals whose *b* axes point along the cylinder length are favored during crystal growth and dominate the structure. The materials which displayed the highest degree of crystal stem alignment were E/MB44 FC and E/MB63 SC. While there was a substantially disparate crystallization time for the two ($t_{1/2} \approx 0.7$ min for E/MB44 versus $t_{1/2} \approx 5$ min for E/MB63, see Table 2), the shorter length of the E/MB44 chains compensates for the shorter crystallization time. A second group of materials—E/MB44 Q, E/MB63 FC, and E/MB88 SC—also displayed stem orientation normal to the cylinder axis, but the alignment was less perfect than that in E/MB44 FC and E/MB63 SC. As the molecular weight of the E/MB increased, progressively slower crystallization was required to produce a similar degree of chain orientation: $t_{1/2} < 0.1$ min for E/MB44 Q, $t_{1/2} \approx 0.6$ min for E/MB63 FC, and $t_{1/2} \approx 5$ min for E/MB88 SC (see Table 2). When chain diffusion is too slow, as in E/MB88 FC and especially in the vitreous E/VCH36, tilt of the crystal stems occurs. The increased area per stem provided by this tilting allows easier accommodation of noncrystalline material at the crystallite surface.

Acknowledgment. Support for this work was provided by the National Science Foundation, Polymers Program (Grants DMR-9257565 and DMR-9711436), and the George Van Ness Lothrop Fellowship from Princeton University (D.J.Q.). The authors gratefully acknowledge the experimental assistance of David Dean (2D X-ray scattering) and Lynn Loo (hydrogenation of the E/VCH36 precursor). In particular, the authors wish to thank Dr. Anuj Bellare (Harvard Medical School) and Professor Robert E. Cohen (Massachusetts Institute of Technology) for their thorough pole figure analysis of samples E/MB44 FC and E/VCH36 VSC.

References and Notes

(1) Rangarajan, P.; Register, R. A.; Fetters, L. J. *Macromolecules* **1993**, *26*, 4640.

(2) Rangarajan, P.; Register, R. A.; Adamson, D. H.; Fetters, L. J.; Bras, W.; Naylor, S.; Ryan, A. J. *Macromolecules* **1995**, *28*, 1422.
(3) Ryan, A. J.; Hamley, I. W.; Bras, W.; Bates, F. S. *Macromolecules* **1995**, *28*, 3860.
(4) Rangarajan, P.; Register, R. A.; Fetters, L. J.; Bras, W.; Naylor, S.; Ryan, A. J. *Macromolecules* **1995**, *28*, 4932.
(5) Nojima, S.; Kato, K.; Yamamoto, S.; Ashida, T. *Macromolecules* **1992**, *25*, 2237.
(6) Quiram, D. J.; Register, R. A.; Marchand, G. R. *Macromolecules* **1997**, *30*, 4551.
(7) Quiram, D. J.; Register, R. A.; Marchand, G. R.; Ryan, A. J. *Macromolecules* **1997**, *30*, 8338.
(8) Yang, Y.-W.; Tanodekaew, S.; Mai, S.-M.; Booth, C.; Ryan, A. J.; Bras, W.; Viras, K. *Macromolecules* **1995**, *28*, 6029.
(9) Douzinas, K. C.; Cohen, R. E. *Macromolecules* **1992**, *25*, 5030.
(10) Hamley, I. W.; Fairclough, J. P. A.; Terrill, N. J.; Ryan, A. J.; Lipic, P. M.; Bates, F. S.; Towns-Andrews, E. *Macromolecules* **1996**, *29*, 8835.
(11) Hamley, I. W.; Fairclough, J. P. A.; Ryan, A. J.; Bates, F. S.; Towns-Andrews, E. *Polymer* **1996**, *37*, 4425.
(12) Cohen, R. E.; Bellare, A.; Drzewinski, M. A. *Macromolecules* **1994**, *27*, 2321.
(13) Craven, J. R.; Hao, Z.; Booth, C. *J. Chem. Soc., Faraday Trans.* **1991**, *87*, 1183.
(14) Ishikawa, S.; Ishizu, K.; Fukutomi, T. *Eur. Polym. J.* **1992**, *28*, 1219.
(15) Ryan, A. J.; Fairclough, J. P. A.; Hamley, I. W.; Mai, S.-M.; Booth, C. *Macromolecules* **1997**, *30*, 1723.
(16) Rangarajan, P.; Haisch, C. F.; Register, R. A.; Adamson, D. H.; Fetters, L. J. *Macromolecules* **1997**, *30*, 494.
(17) Cohen, R. E.; Cheng, P. L.; Douzinas, K.; Kofinas, P.; Berney, C. V. *Macromolecules* **1990**, *23*, 324.
(18) Viras, K.; Viras, F.; Campbell, C.; King, T. A.; Booth, C. *J. Chem. Soc., Faraday Trans. 2* **1987**, *83*, 917.
(19) Yeates, S. G.; Booth, C. *Makromol. Chem.* **1985**, *186*, 2663.
(20) Quiram, D. J. Ph.D. Thesis, Princeton University, 1997.
(21) Morton, M.; Fetters, L. J. *Rubber Chem. Technol.* **1975**, *48*, 359.
(22) Gehlsen, M. D.; Bates, F. S. *Macromolecules* **1993**, *26*, 4122.
(23) Adams, J. L.; Quiram, D. J.; Graessley, W. W.; Register, R. A.; Marchand, G. R. *Macromolecules* **1998**, *31*, 201.
(24) Adams, J. L.; Quiram, D. J.; Graessley, W. W.; Register, R. A.; Marchand, G. R. *Macromolecules* **1996**, *29*, 2929.
(25) Brandrup, J., Immergut, E. H., Eds. *Polymer Handbook*, 3rd ed.; Wiley: New York, 1989.
(26) Krishnamoorti, R. Ph.D. Thesis, Princeton University, 1994.
(27) Howard, P. R.; Crist, B. *J. Polym. Sci., B: Polym. Phys.* **1989**, *27*, 2269.
(28) Reichart, G. C. Ph.D. Thesis, Princeton University, 1997.
(29) Khan, S. A.; Larson, R. G. *Rheol. Acta* **1991**, *30*, 1.
(30) Lee, H. H.; Register, R. A.; Hajduk, D. A.; Gruner, S. M. *Polym. Eng. Sci.* **1996**, *36*, 1414.
(31) Tepe, T.; Schulz, M. F.; Zhao, J.; Tirrell, M.; Bates, F. S.; Mortensen, K.; Almdal, K. *Macromolecules* **1995**, *28*, 3008.
(32) Keith, H. D.; Padden, F. J., Jr.; Vadimsky, R. G. *J. Polym. Sci.* **1966**, *4*, 267.
(33) Kakudo, M.; Kasai, N. *X-Ray Diffraction by Polymers*; Elsevier: New York, 1972.
(34) Alexander, L. E. *X-Ray Diffraction Methods in Polymer Science*; Krieger: Malabar, FL, 1985.
(35) Stack, G. M.; Mandelkern, L.; Voigt-Martin, I. G. *Macromolecules* **1984**, *17*, 321.
(36) Voigt-Martin, I. G.; Mandelkern, L. *J. Polym. Sci.: Polym. Phys. Ed.* **1984**, *22*, 1901.
(37) Voigt-Martin, I. G. *Adv. Polym. Sci.* **1985**, *67*, 196.
(38) Song, H. H.; Roe, R.-J. *Macromolecules* **1987**, *20*, 2723.

MA971218H